Int J Thermophys (2015) 36:880–890
DOI 10.1007/s10765-014-1773-3

Combined Photoacoustic Ultrasound and Beam Deflection Signal Monitoring of Gold Nanoparticle Agglomerate Concentrations in Tissue Phantoms Using a Pulsed Nd:YAG Laser

Mohammad E. Khosroshahi · Andreas Mandelis

Received: 2 December 2013 / Accepted: 17 October 2014 / Published online: 6 November 2014

Abstract The purpose of this paper is to show and discuss the effects of the gold nanoparticle (Au-NPs) concentration inside a tissue phantom using a combined system of photoacoustics (PA) and optical beam deflection and their applications particularly to photoacoustic imaging. It was found that the PA signal from aggregated Au nanoparticles is significantly enhanced. The stock concentration of 100 nm Au-NPs was 3.8×10^9 particles/mL from which three samples with 30 %, 70 %, and 90 % concentration were prepared using polyvinyl chloride-plastisol. Each sample was then irradiated across a line scan using a 10 ns pulsed Q-switched Nd:YAG laser at a 1 Hz repetition rate and 5 $W \cdot cm^{-2}$ so that no physical ablation was observed. The corresponding photoacoustic pressure was found to approximately cover a range between 10 kPa and 51 kPa. This corresponds to approximately 130 pJ to 315 pJ of acoustic energy radiated by Au-NPs into the tissue. The maximal efficacy of the transformation of optical energy into thermal energy was ∼29 %. Time-resolved photoacoustic deflection was also used to monitor the laser-interaction process. The results clearly indicated that (i) the photoacoustic signal amplitude varies in a given sample as a result of the non-uniform concentration distribution of embedded Au-NPs; (ii) an increase of the concentration increased the signal amplitude linearly; and (iii) at higher nanoparticle concentrations, the probe deflection was found to increase due to a steeper thermoelastic gradient as a result of a higher absorption by particle agglomerates and particle size-dependent dispersions.

M. E. Khosroshahi · A. Mandelis
Center for Advanced Diffusion-Wave Technologies, Department of Mechanical and Industrial Engineering, University of Toronto, Toronto, ON M5S 3G8, Canada

M. E. Khosroshahi (✉)
Faculty of Biomedical Engineering, Biomaterial Group, Laser & Nanobiophotonics Laboratory, Amirkabir University of Technology, Tehran, Iran
e-mail: khosrom@mie.utoronto.ca

Keywords Biomedical photoacoustics · Gold nanoparticles · Nd:YAG laser · Photoacoustic beam deflection

1 Introduction

In recent years growing interest has been shown in developing new techniques for the non-invasive monitoring and imaging of biomedical structures and tissues. Optical scattering in soft tissue degrades the resolution significantly with depth while ultrasound can provide a better resolution than optical means for depths greater than about 1 mm. Thus, the combination of high optical absorption contrast and high ultrasonic spatial resolution (low scattering) makes it a very useful imaging technique. Basically, photoacoustics (PA) is a material probing modality in which the absorption of incident pulsed laser radiation leads to impulsive heating of the irradiated tissue volume, followed by rapid thermoelastic expansion and subsequent generation of broadband ultrasonic thermoelastic waves [1]. Equally, the photothermal deflection (PTD) is based on the localized heating of a sample by a focused laser source acting as a "thermal piston." Rapid heating is then transferred to air molecules in the vicinity of the surrounding gas producing a temperature gradient field which is effective when the beam passing through this heated region is deflected by the thermally modulated index of the refraction gradient. The amplitude and phase of the deflected beam carry some information about optical and thermophysical properties of the solid or liquid, thereby enabling a number of biomedical applications by both techniques [2,3]. In this manner, one can obtain a better contrast and spatial resolution of tissue images [4]. Despite much valuable research work regarding PA imaging [5–7], a further enhancement of photoacoustic (or optoacoustic) imaging contrast would be necessary for the early detection of cancer at deep subsurface locations. Gold nanoparticles (Au-NPs) exhibit unique optical properties, namely, strong localized surface plasmon resonance (LSPR) which is defined as a collective and coherent oscillation of conduction electrons when excited by an external source of an electromagnetic field. As a consequence of the plasmon oscillation, a dipolar is generated with a huge enhancement of the local electric field at the nanoparticles surface. This electric field leads to strong light absorption and scattering at the SPR frequency by the particle [8–10], and their major advantages are biocompatibility due to their inert surface, nontoxicity, surface conjugation chemistry, and lack of photobleaching or blinking as with quantum dots [11,12]. Besides, Au-NPs are relatively simple to synthesize, and they are photostable and can be easily conjugated with proteins, antibodies, and specific cancer ligands [13,14]. Thus, they have been chosen for bioimaging [15,16], mainly due to their ability to convert absorbed light into heat (i.e., PA efficiency) [17], drug delivery [18,19], cancer cell diagnosis and therapeutics [20,21], and laser tissue welding and soldering [22,23]. Above all, since cellular uptake and endocytosis of particles results in their aggregation, it also has a significant impact on the application of plasmonic metal nanoparticles for molecular imaging. The goal of this paper is to study the effects of the gold NP concentration on PA signals using a Q-switched pulsed Nd:YAG laser and simultaneously monitoring the interaction process based on photoacoustic deflection signals.

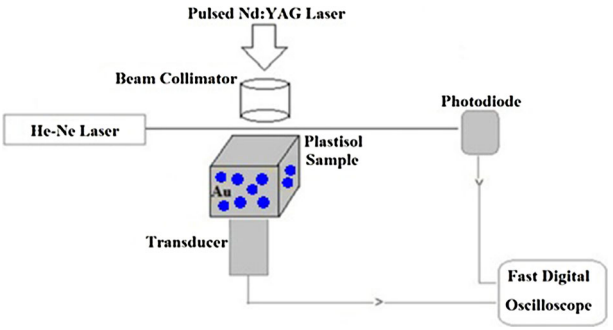

Fig. 1 Experimental setup for simultaneous PA ultrasound and laser beam deflection measurements

2 Experimental

2.1 Materials

To study the effects of the Au-NP concentration on photoacoustic signals, a tissue phantom made of polyvinyl chloride-plastisol (PVCP), a non-toxic plastic synthesized from chloride monomers and soluble in water was purchased from M-F Manufacturing Co., Fort Worth, TX, USA. PVCP is a viscoelastic material and its creep deformation is very low compared with other plastics due to its limited molecular motion at ordinary temperatures. For these types of materials, the relationship between stress and strain depends on time and the stiffness will depend on the rate of the applied load. In addition, the mechanical energy is dissipated by conversion of heat in the deformation of viscoelastic materials. The solution is an oil-based liquid and was uniformly heated and stirred continuously using a magnetic stirrer up to ≈200 °C in order to avoid structural and optical inhomogeneities and then allowed to cool. It has no or very negligible optical absorption at a 1.06 μm wavelength of an Nd:YAG laser and has a similar speed of sound (1400 $m \cdot s^{-1}$) and density as tissue and makes a suitable candidate for modeling tissue biomedical applications [24]. A 25 mL gold nanoparticle (Au-NP) source with 100 nm diameter and a concentration of 3.8×10^9 particles/mL (i.e., 9.5×10^{10} particles) stabilized as a suspension in a citrate buffer was purchased from Sigma-Aldrich. Three samples were prepared by injecting 0.3 mL, 0.7 mL, and 0.9 mL of Au-NPs in 1 cm^3 of PVCP solution. Upon cooling, the solution was solidified and was easily removed from the container.

2.2 Method

The experimental setup is shown in Fig. 1. Each sample was irradiated using a 10 ns pulsed Q-switched Nd:YAG laser (Continum-Surelite) at a 1.064 μm wavelength with a 1 mm collimated pulse at 1 Hz and 5 $W \cdot cm^{-2}$ intensity. The thermoelastic signals were detected by a 2.2 MHz focused transducer (V305,Olympus NDT Inc., Panametrics) with 18.8 mm diameter and 25 mm focal length, and were then recorded with a fast digital oscilloscope (Tektronix-DPO 7104-1 GHz).

A 2 mW He-Ne laser (632 nm) was used as a probe beam for photoacoustic deflection measurements. The beam was focused with a lens of 100 mm focal length to a diameter of about 0.5 mm. The dependence of the photodiode response ΔV on the beam deflection is [25]

$$\Delta V = V_0 \operatorname{erf}\left[2^{1/2}\varphi/\theta\right] \tag{1}$$

with φ and θ being the beam angular deflection due to changes in refraction and angular divergence, respectively. Also, the thermally or PA pressure-induced optical deflection, φ, is directly related to the rate of change of the refractive index and the temperature

$$\varphi = \frac{1}{n}\frac{\partial n}{\partial T}\frac{\partial T}{\partial z}L, \tag{2}$$

where n is the refractive index, T is the temperature, and L is the probe beam path. It is interesting to note that since pure plastisol (i.e., without impurities) acts as a weakly absorbing material for an Nd:YAG laser, the temperature in Eq. 1 is mainly due to absorption by Au-NPs. The temperature of a single NP is given by Eq. 3 where it increases linearly with absorbed power but is inversely related to the medium thermal conductivity, $K_\mathrm{p}(=D_\mathrm{p}\rho_\mathrm{p}c_\mathrm{p})$ with ρ_p, c_p, and D_p being the density, specific heat capacity, and the thermal diffusivity of the NP, respectively [26].

$$\Delta T = \frac{P}{4\pi R_\mathrm{p} K_\mathrm{p}} \tag{3}$$

where P is the laser power and R_p is the NP radius. Thus, the larger is the sphere, the longer it takes for heat to diffuse or transfer to the surrounding medium (i.e., it cools slowly at a longer time). In fact, both PA and PTD are observable with the same setup except that PA deflections occur on a much earlier time scale. The output signal was then registered using a Si-based photodiode (Thorlabs-DET10A) with a spectral sensitivity between 200 nm and 1100 nm. In combining PA ultrasound detection with a conventional transducer and PA beam deflection, some additional sample information can be obtained, such as the sound velocity, elasticity, temperature, flow velocity, thermal diffusivity, and thickness. In the case of viscoelasticity, if we assume a knowledge of the tensile stress, σ, and differentiating it with respect to x,

$$\begin{aligned} \sigma &= E_\mathrm{y}[\varepsilon_0 - \beta T\,(x,t)] \\ \frac{\partial\sigma}{\partial x} &= E_\mathrm{y}\left[\frac{\partial\epsilon}{\partial x} - \beta\frac{\partial T}{\partial t}\,(x,t)\right], \end{aligned} \tag{4}$$

where $E_\mathrm{y} = \sigma/\varepsilon_0$ is the Young's modulus, $\varepsilon_0 = \partial u/\partial x$ is the strain or the displacement of a particle in the x-direction, $\beta = \frac{\Delta P C_\mathrm{p}}{c_\mathrm{a}^2 \alpha F}$ represents the volumetric thermal expansion, ΔP is the pressure increase due to volume expansion, C_p is the specific heat capacity,

c_a is the acoustic velocity in the material, α is the material absorption coefficient, and F is the laser fluence. Since $T(x,t) = \alpha \int_0^t \frac{I\,dt}{\rho C_p}$

$$\frac{\partial T}{\partial x} = \frac{\alpha}{\rho C_p}\frac{\partial \int_0^t I\,dt}{\partial x} = \frac{1}{C_p}\partial W/\partial x \tag{5}$$

where $W = \frac{\alpha}{\rho C_p}\int_0^t I\,dt$ is the absorbed energy per unit volume. Using Newton's second law of motion, we obtain

$$\frac{\partial^2 u}{\partial t^2} = \frac{1}{\rho}\frac{\partial \sigma}{\partial x} \tag{6}$$

Substituting Eqs. 4 and 5 into Eq. 6 and simplifying,

$$\begin{aligned}\frac{\partial^2 u}{\partial x^2} - \frac{1}{c_a}\frac{\partial^2 u}{\partial t^2} &= \frac{\beta}{C_p}\frac{\partial W}{\partial x}\\ \frac{\partial^2 u}{\partial x^2} - \frac{1}{c_a}\frac{\partial^2 u}{\partial t^2} &= \frac{\Delta P}{c_a^2}\frac{1}{\alpha F}\frac{\partial W}{\partial x}.\end{aligned} \tag{7}$$

It can be seen from Eqs. 5 and 7 that the rate of change of temperature is directly related to the absorption coefficient of the material and the laser intensity and, hence, to the optical deflection, φ. Secondly, for an unknown material, the value of $(E_y/\rho)^{1/2}$ can be deduced using the experimental value of the acoustic propagation velocity (i.e., $c_a = (E_y/\rho)^{1/2}$).

3 Results and Discussion

The amplitude of our bipolar thermoelastic signals increased approximately linearly with increasing Au-NP concentration, as expected from linear photoacoustic theory. Some examples of PA thermoelastic responses are shown in Fig. 2a and b. The increasing trend of the average PA amplitude with Au concentration at a constant power density is illustrated in Fig. 2c. The peak output voltage from the transducer can be converted to a corresponding normal force and hence to a pressure (= F/A, Pa) if the irradiated area, A, is known. From the known voltage amplitude, V, and other constants of the PZT transducer, the corresponding values of the average photoacoustic pressure can be found using $P = CV(t)/d_t A$ where $C = (C_l + C_d \approx 10^{-9}\text{F})$ is the sum of load and transducer capacitances and $d_t \approx 10^{-12}\,\text{pC}\cdot\text{N}^{-1}$ is the strain constant. Thus, it was found from the measured amplitudes that the corresponding calculated acoustic pressure covered the range between 10 kPa and 51 kPa.

The narrowing of the pressure transient $FWHM$, Δt, with concentration at a constant power density, Fig. 2b, can be explained by considering the simple relation (Eq. 8) below which relates the acoustic energy, ΔE_a, delivered to the tissue to the pulse peak pressure, P_0, and Δt through [27]

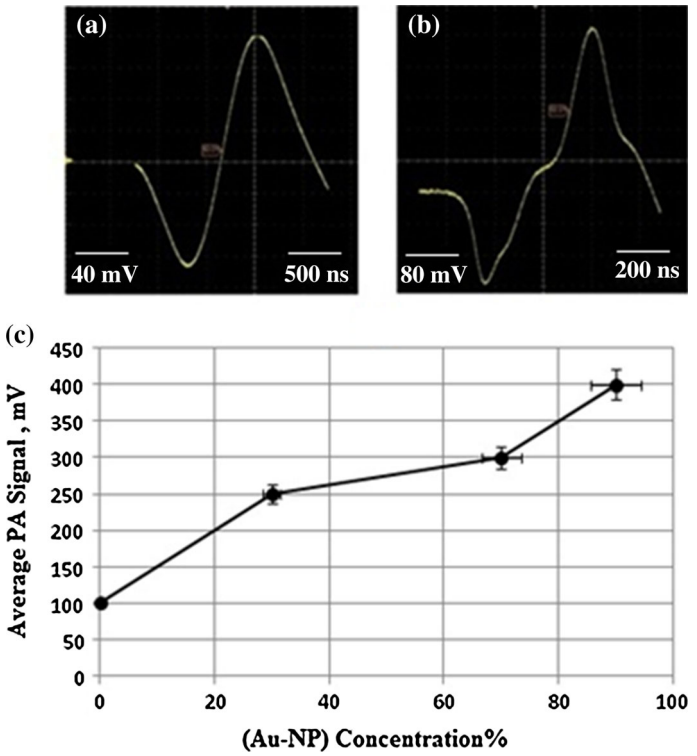

Fig. 2 Examples of some typical thermoelastic signals for 30 % of Au-NPs: (a) 160 mV, 550 ns, (b) 70 %: 400 mV, 160 ns, and (c) PA signal variation with NP concentration

$$\Delta E_{\mathrm{a}} \approx P_0^2 A \Delta t / \rho c_{\mathrm{a}} \tag{8}$$

Thus, the peak value of the pressure (P_0) is directly proportional to $\Delta t^{-1/2}$ under conditions of a fixed acoustic energy which, in practice, means a decrease in the transient pulse duration is compensated by increasing the pressure. The pressure itself is, of course, directly proportional to the laser fluence in the linear regime. Therefore, taking the value of the PVCP density close to that of the soft tissue, $\rho \approx 1000\ \mathrm{kg \cdot m^{-3}}$ and the acoustic velocity of about $1400\ \mathrm{m \cdot s^{-1}}$ using [14], the area of irradiation, $A \approx 7.85 \times 10^{-3} \mathrm{cm}^2$, and then by substituting the experimental values of the acoustic pressure (10 to 51) kPa and the pressure pulse widths measured at full width half maximum in Eq. 8, the amount of acoustic energy delivered to the tissue without and with nanoparticles is approximately determined as 45 pJ and (130 and 315) pJ, respectively. Figure 3a shows the PA signal waveforms detected by the transducer, and Fig. 3b indicates the PA-induced probe beam deflection detected by the photodiode at the relatively high concentration of 70 % of Au-NPs, equivalent to 26 $\mu\mathrm{g \cdot mL^{-1}}$, where rapid heating, as a result of absorption of laser radiation by the sample, generates fast thermoelastic expansion followed by deep rarefaction due to various non-radiative excitation processes occurring inside the PVCP. Our results are similar and comparable

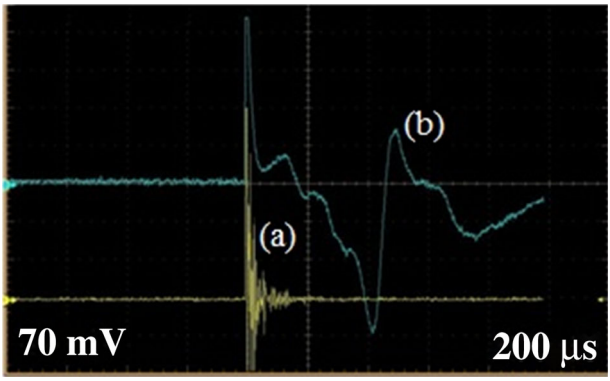

Fig. 3 (a) Typical photoacoustic signal detected by transducer and (b) photoacoustic probe beam deflection waveforms detected from the surface of the tissue phantom

with those of Sell et al. [28], and they suggested that polarities of the deflection signal are consistent with the evolution of a shock wave from a sound wave. When this occurs, the negative leading edge tends to shorten and steepen, while the positive shock's wave edge broadens. Although there is no agreed-upon value for a safety threshold (it varies case by case), the concentration used in this experiment is almost half the amount ($56\ \mu g \cdot mL^{-1}$) used by Bayer et al. [29] and Sun et al. [30] for PA imaging of drug release.

Using the expression for the nanoparticle thermal diffusion length, $X_T = (D_p \tau_p)^{1/2}$ where τ_p is the laser pulse duration, we can assume the NP volume was heated during the laser pulse action because R_p (50 nm) $<<$ $X_T \approx 1\ \mu m$, and for gold NPs, $D_p \approx 1.2 \times 10^{-4}\ m^2 \cdot s^{-1}$ [31]. Similarly, the thermal diffusion length delivered by the NPs in tissue would be $(D_t \tau_p)^{1/2} \approx 4\ \mu m$, taking $D_t \approx 1.3 \times 10^{-3}\ cm^2 \cdot s^{-1}$ [32]. Now, the following equation is used to determine the characteristic thermal relaxation time for nanoparticles with a radius, R_p [33]:

$$\tau_r = \rho_p c_p R_p^2 / 3K_p \tag{9}$$

With $\rho_p \approx 19.3\ g \cdot cm^{-3}$ and $c_p \approx 0.13\ J \cdot g^{-1} \cdot °C^{-1}$, Eq. 9 yields $\tau_r \approx 7$ ps $<<$ $\tau_p \approx 10$ ns [34,35]. Therefore, in our case, $\tau_p >> \tau_r$, and we have a non-adiabatic situation where no thermal confinement is achieved within a nanoparticle and there is heat exchange between NP and tissue. Our findings are in close agreement with Bayer et al. [29] where PA signals from an agglomeration were stronger than from monodisperse NPs. This is so because the PA signal is sensitive to the heat transfer properties of embedded nanoparticles relative to their surroundings; therefore, it is expected that changes to the temporal and spatial characteristics of heat transfer due to aggregation lead to a signal increase which is linked to the thermal properties and thermodynamics of the nanoparticle-surroundings system [29,36]. In terms of energy, the PA signal is insensitive to the scattering effect because the PA signal is determined by the absorbed fraction of the incident optical energy that is converted to heat. However, the photon density distribution of light changes when it is scattered.

This causes a change in the heated region and introduces a change in the shape of the sound source.

While optical absorption depends on the material type, scattering is caused by the inhomogeneity in the refractive index of a medium and the spatial distribution of the scattering depends on the size and shape of the inhomogeneity relative to the source wavelength. It is known that for a turbid medium, the reduced scattering coefficient, $\beta' = \beta(1 - g)$, where β is the scattering coefficient and g is the anisotropy factor or the mean cosine of the scattering which varies between -1 and 1. Since, in our case, $R_p \approx 50$ nm $\leq \lambda/20 \approx 53$ nm and $x = 2\pi R_p/\lambda \approx 0.3 < 1$; thus, Rayleigh scattering can be assumed when $g = 0$. However, when the particle size increases due to, for example, NP clustering, the intensity distribution increases in the forward direction, $g = 1$, and the scattering phase function, $p(\hat{a}, \hat{s}')$ for small angles becomes much higher than for all other angles. The minimum value of $g = -1$ indicates backward scattering. $p(\hat{s}, \hat{s}')$ describes the fraction of light energy incident on the scatterer from the $\hat{s}'$ direction that gets scattered in the new direction $\hat{s}$.

However, it must be emphasized that the concept, and hence the effects of agglomeration or clustering under optical interaction irradiation, are different from the situation where high numbers of single particle dispersions exist within the medium. This can further be understood and clarified by noting that basically, the agglomeration process for colloidal particles results from the coupling between two main interactions: (1) particle-fluid interactions, which play a role in the motion of particles within a flow and govern the number of particle–particle encounters, and (2) particle–particle interactions, which control whether colliding particles will adhere (adhesion or attractive interaction) or simply bounce (repulsive interaction). The second process, as in this case, is described by the DLVO (Derjaguin, Landau, Verwey, and Overbeek) theory [37,38] which defines inter-particle forces as the sum of van der Waals and double-layer electrostatic contributions. Taking this idea into consideration, it then can be assumed that the number of spherical solid particles (N_{NP}) dispersed in a medium (analogous to the Gibbs energy) is proportional to the change of average particle diameter (D), equivalent to the coordination number, at any time (t),

$$N_{NP} = P\,(D_{max} - D)\,, \tag{10}$$

where D_{max} is the maximum diameter that particles can reach when a minimum number of particles remain in the dispersion and P is a proportionality constant that takes into account the shape factor of the particles. The variation of the number of particles with respect to time due to agglomeration is [39]

$$-\,\mathrm{d}N_{NP}/\mathrm{d}t = kN^n. \tag{11}$$

Here, k is the agglomeration rate coefficient, and n is the reaction order and deriving Eq. 10:

$$\mathrm{d}N_{NP} = -Pd\,(D)\,. \tag{12}$$

Substituting Eq. 10 into Eqs. 12 and 11,

$$P\frac{\mathrm{d}(D)}{\mathrm{d}t} = k\left[P\left(D_{\max} - D\right)\right]^{n}. \tag{13}$$

Considering $n = 1$ [40],

$$\frac{\mathrm{d}(D)}{\mathrm{d}t} = k\left(D_{\max} - D\right). \tag{14}$$

If at $t = 0$, $D = D_0$, then Eq. 14 becomes

$$D = D_{\max} - \exp\left(-kt\right)\left(D_{\max} - D_0\right), \tag{15}$$

where D_0 is the initial particle diameter at $t = 0$.

Dividing the equation by D_0 and rearranging, we obtain

$$d = d_{\mathrm{eq}} - \exp\left(-kt\right)\left(d_{\mathrm{eq}} - 1\right), \tag{16}$$

where $d = D/D_0$ and $d_{\mathrm{eq}} = D_{\max}/D_0$. Equation16 represents the behavior of the particle diameter as a function of time for $n = 1$. The agglomeration rate, k, is a function of temperature. The calculation of the activation energy is necessary to determine the nature of the agglomeration process. Now, it is well known that quantitative PA imaging in the presence of nanoparticles is based on the linearity of the PA signal (maximum signal voltage, $V_{\max}$), and on the number of nanoparticles (N_{NP}) with a wavelength-dependent optical absorption cross section, $\sigma(\lambda)$, in the illuminated volume with fluence F, and on the deposited energy (σF). This relationship is given as

$$V_{\max}(F) - V_0(F) \propto \Gamma_{\mathrm{eff}}\sigma(\lambda) N_{\mathrm{NP}} F, \tag{17}$$

where Γ_{eff} is the effective Grüneisen constant for a given NP in a non-absorbing solvent and V_0 is the PA signal from any endogenous absorbers. This relation holds as long as the NP absorption cross section and environment are constant, and particle-to-particle thermal and electromagnetic coupling can be neglected. If V_0 is negligible, then $V_{\max}$ results from the NPs only and $\Gamma_{\mathrm{eff}}\sigma(\lambda)$ is a constant that can be measured independently. Based on Eq. 17, the PA signal was increased by increasing the Au-NP concentration.

4 Conclusion

PA and photoacoustic beam deflection (PABD) were applied simultaneously for the first time as a combined modality for monitoring the distribution of the nanoparticle concentration within a tissue phantom and also for the study of nanoparticle effects on the ultrasound signal. The increase in the PA signal amplitude in relation to the concentration of Au-NPs was quantitatively demonstrated which in turn has a direct

effect on the imaging quality. The effect of 100 nm Au nanoparticle concentration on the pulsed Nd:YAG laser-induced PA ultrasonic and PA deflection signals was studied using PVCP as a phantom tissue. A non-adiabatic condition was obtained where a thermal exchange took place between the tissue phantom and Au-NPs. Based on Eq. 17, the PA signal was increased by increasing the Au-NP concentration and at a constant Au concentration. PABD which is based on density variations in the vicinity of the solid surface followed by a refractive-index gradient in the medium indicated an optoacoustic wave propagation and acoustic density gradients due to absorption by NPs. The results further imply the potential for improved biomedical PA imaging contrast using nanoparticle agglomerates or a high number of monodispersions. Because cellular uptake and endocytosis of particles results in their aggregation, it also has significant impact on the application of plasmonic metal nanoparticles for molecular imaging. Also, capitalizing on the Doppler shift in the plasmon resonance frequency of Au-NPs due to specific molecular aggregation, PA can be used for selective imaging. A multi-wavelength PA imaging system is thought to quantitatively indicate spectral variations in the optical absorption properties of tissue; therefore, it can differentiate between the distribution of endogenous and exogenous contrast agents.

References

1. A. Tam, Rev. Mod. Phys. **58**, 381 (1986)
2. P.E. Dyer, in *Photoacoustic and Photothermal Phenomena, Springer Series in Optical Sciences*, ed. by P. Hess, J. Pelzl, vol. 58 (Springer-Verlag, Berlin, 1988), p. 164
3. M.E. Khosroshahi, A. Ghasemi, Lasers Med. Sci. **18**, 196 (2004)
4. D. O'Neal, L. Hirch, N.J. Halas, Cancer Lett. **209**, 171 (2004)
5. R. Esenaliev, A. Karabutov, A. Oraevsky, IEEE J. Quan. Electron. **5**, 186 (1999)
6. P.C. Beard, Proc. SPIE **4618**, 54 (2002)
7. S. Telenkov, A. Mandelis, J. Biomed. Opt. **14**, 044025 (2009)
8. V.K. Pustovalov, V. Babenkov, Laser Phys. Lett. **10**, 516 (2004)
9. O. Govorov, H.H. Richardson, Nano Today **1**, 30 (2007)
10. Z. Hasannejad, M.E. Khosroshahi, Opt. Mater. **35**, 644 (2013)
11. C. Weibo, G. Ting, H. Hao, S. Jiangto, Nanotech. Sci. Technol. **1**, 17 (2008)
12. M.E. Khosroshahi, M. Nourbakhsh, Lasers Med. Sci. **26**, 49 (2011)
13. R. Sinha, G.J. Kim, S. Nie, D.M. Shin, Mol. Cancer Ther. **5**, 1909 (2006)
14. M.E. Khosroshahi, L. Ghazanfari, Mater. Chem. Phys. **133**, 55 (2012)
15. Q. Zhang, N. Iwakuma, B. Moudgil, C. Wu, Nanotechnology **20**, 1 (2009)
16. A. Sajjadi, A. Suratkar, K. Mitra, J. Nanotech, Eng. Med. (ASME) **3**, 1 (2012)
17. V.K. Pustovalov, L.G. Astafyeva, E. Galanzha, V.P. Zharov, Cancer Nanotechnol. **1**, 35 (2010)
18. A.A. Kuznetsov, V.I. Filippov, R.N. Alyautdin, N.L. Torshina, O.A. Kuznetsov, J. Magn. Magn. Mater. **225**, 95 (2001)
19. M. Mahmoodi, M.E. Khosroshahi, F. Atyabi, J. Biophotonics **6**, 403 (2011)
20. J.B. Wolinsky, M.W. Grinstaff, Adv. Drug Del. Rev. **60**, 1037 (2008)
21. Ch. Patra, R. Bhttacharya, D. Mukhopadhyay, P. Mukherjee, Adv. Drug. Del. Rev. **62**, 346 (2010)
22. A.M. Gobin, D.P. O'Neal, D.M. Watkins, N.J. Halas, R.A. Drezek, J.L. West, Lasers Surg. Med. **37**, 123 (2005)
23. M.E. Khosroshahi, M. Nourbakhsh, J. Biomed. Opt. **16**, 088002 (2011)
24. G. Spirou, A. Oraevsky, I. Vitkin, W. Whelan, Phys. Med. Biol. **50**, N142 (2005)
25. J. Diaci, J. Mozina, Appl. Phys. A **55**, 84 (1992)
26. B. Falsa, A.R. Senoudi, A. Boussaid, M. Benmouna, R. Benmouna, J. Biomater. Nanobiotechnol. **2**, 49 (2011)
27. P. Dyer, M.E. Khosroshahi, S. Tuft, Appl. Phys. B. **56**, 84 (1993)
28. J.A. Sell, D. Heffelfinger, P. Ventzek, R. Gilgenbach, J. Appl. Phys. **69**, 1330 (1991)

29. C. Bayer, S. Yun Nam, Y. Chen, J. Biomed. Opt. **18**, 016001 (2013)
30. Y. Sun, K.C.P. King, B. O'Neill, Proc. SPIE **8581**, 85813F-1 (2013)
31. G. Lopez-Munoz, J. Pescador-Rojas, Nanoscale Res. Lett. **7**, 423 (2012)
32. J.T. Walsh Jr, J.P. Cummings, Proc. SPIE **1202**, 12 (1990)
33. V. Pustovalov, L. Astafyevea, E. Galanzha, Cancer Nano. **1**, 35 (2010)
34. American Institute of Physics, *American Institute of Physics Handbook* (McGraw-Hill Press, New York, 1972)
35. V.K. Pustovalov, Chem. Phys. **308**, 103 (2005)
36. J. Shah, S. Park, S. Aglyamov, T. Larson, L. Ma, K. Sokolov, K. Johnston, T. Milner, S. Emelianov, Proc. SPIE **6856**, 68560U–1 (2008)
37. B. Derjaguin, L. Landau, Acta Physicochim. URSS **14**, 633 (1941)
38. E. Verwey, J. Overbeek, *Theory of Stability of Lyophobic Colloides* (Elsevier Press, Amesterdam, Netherlands, 1948)
39. H. Loria, P. Pereira-Almao, C. Scott, Ind. Eng. Chem. Res. **50**, 8529 (2011)
40. J. Thompson, J. Vasquez, J. Hill, P. Pereira-Almao, Ind. Eng. Chem. Fundam. **123**, 16 (2008)